EUROPEAN JOURNAL OF PURE AND APPLIED MATHEMATICS
2025, Vol. 18, Issue 4, Article Number 6968
ISSN 1307-5543 – ejpam.com
Published by New York Business Global

Bifurcations, Hidden Attractors, and Chaos in a Nonlinear Three-Dimensional System

Hafidh Khoerul Fata[1], Nurcahya Yulian Ashar[1,*]

[1] *Department of Mathematics, Faculty of Science and Mathematics, Universitas Diponegoro, Semarang, 50275, Indonesia*

Abstract. This research shows an analytical and numerical analysis of a nonlinear three-dimensional dynamical system controlled by a unique control parameter, named α. The system exhibits self-excited oscillations through local bifurcations for negative α, including saddle-node and supercritical Hopf bifurcations, leading to periodic orbits and a sequence of period-doubling transitions into chaos. On the other hand, when α is negative and there are no equilibrium points, the system shows long term oscillations that last for a long time through hidden attractors—bounded chaotic dynamics with basins of attraction that are not connected to any equilibrium. Numerical continuation and Lyapunov spectrum analysis confirm the simultaneous existence of periodic, quasiperiodic, and chaotic regimes. The results demonstrate the intricate interplay between local bifurcations and global nonlinear frameworks, emphasizing the distinctive routes to chaos and the emergence of hidden dynamics in systems lacking stability.

2020 Mathematics Subject Classifications: 34C23, 34C28, 34D45, 37G10

Key Words and Phrases: Hidden chaos, period-doubling bifurcation, nonlinear dynamical systems

1. Introduction

Nonlinear dynamical systems are essential for modeling complex behaviors in physics, biology, engineering, and economics [1–5]. Unlike linear systems, nonlinear systems exhibit sensitivity to initial conditions and parameters, often leading to significant changes in behavior. This sensitivity makes rise to phenomena such as double equilibria, limit cycles, bifurcations, quasi-periodicity, and chaos [6]. Knowing how system structure evolves with parameters is very important for forcasting and mantaining long-term dynamics.

To study about nonlinear phenomena gives practical insights across fields such as population dynamics [7], electronic circuits [8], climate change variability [9], and mechanical vibrations [10]. A prime objective is to check how parameter changes trigger qualitative

*Corresponding author.
DOI: https://doi.org/10.29020/nybg.ejpam.v18i4.6968

Email addresses: yulian@lecturer.undip.ac.id (N. Y. Ashar)

 Copyright: © 2025 The Author(s). (CC BY-NC 4.0)

shifts—such as movements from stability to chaos—through bifurcations, a essence concept in nonlinear analysis [11]. Chaos theory reveals that deterministic systems can move unpredictable over time, challenging assumptions of control and predictability. Examples include honeybee models presenting nonlinear feedback consequentes [7], Chua oscillators with controllable chaos [8], fractional-delay models of atmospheric influxes [9], and nonlinear trembling responses in railway tools [10].

To check these phenomena, dynamical system analysis generally combines analytical and numerical methods. Local stability and bifurcation analyses, especially in proximity to equilibrium points, can show the importance of oscillatory or unstable dynamics. However, these localized instruments are inadequate for elucidating the complete global dynamics of nonlinear systems. So numerical continuation methods and phase space visualizations are important for elucidating bifurcation structures and global movements, including pathways to chaos [12]. In this methodological context, the textbooks by Kuznetsov [11], Perko [13], and Wiggins [14] establish the theoretical foundation for local analysis. Meanwhile, Ananthkrishnan et al. [15] demonstrate computational multiparameter continuation, and di Bernardo et al. [16] along with Han et al. [17] emphasize the necessity for global tools in nonsmooth or hybrid environments.

Among the many forms of chaotic systems, a particularly interesting subclass is the three-dimensional system with quadratic nonlinearity and no equilibrium [18, 19]. While the analysis of dynamical systems always starts from the equilibrium point, in systems with no equilibrium, the analysis is quite difficult to perform because there are few analytical methods to observe their dynamics. In their foundational work, Jafari et al. [19] introduced a catalog of several such systems, among which the NE12 system exhibits chaos despite the absence of equilibrium points for a certain range of parameters. However, their study only identified the existence of chaotic dynamics of the system using Lyapunov exponents and Kaplan–Yorke dimensions at parameter values where the system had no equilibrium points, without exploring the underlying bifurcation structure or the global evolution of the system dynamics as the parameters varied.

This research addresses the lack of general analysis of the NE12 system by combining analytical and numerical methods. We first see local stability and identify a supercritical Hopf bifurcation at a critical parameter. Using numerical continuation, we check periodic orbits and make global bifurcation structures, including period-doubling cascades and also hidden attractors. Complexity is calculated through largest Lyapunov exponents and also Kaplan–Yorke dimensions, making bifurcation plots and Lyapunov diagrams that map movements between regular and chaotic regimes [20]. Phase-space plots and Poincaré sections display geometric aspects, while Lyapunov exponents are computed using the ancient method of Wolf et al. [20]. The observed dynamics align with known paths to chaos in diverse systems, such as viscoelastic streams [21], photorefractive mixing [22] ultrafast lasers [23], and microbeam oscillations [24], sharping the universality of these mechanisms.

The novelty of this study located in its systematic explanation of the global bifurcation act of the NE12 system, which has not been comprehensively and generally analyzed before. Unlike the original work by Jafari et al.,[19] which explained NE12 as a chaotic

stream with no equilibrium, our joined analytical and numerical approach reveals transitions between stable, periodic, and chaotic dynamics via bifurcation mechanisms. This shows deeper insight into the system's global structure and the interplay between local instabilities and global attractors. Recent advances in hidden attractors in fractional, geometric, and simple three dimension systems [25–28] further clarify the distinction between self-excited dynamics (linked to equilibrium stability) and hidden dynamics (characterized by the lack of equilibrium and unconnected basins).

2. The Model

This reasearch investigates the dynamics of a three-dimensional nonlinear dynamical system originally worked by Jafari et al. [19], which exhibits chaotic act below nonequilibrium conditions. The system is governed by the following set of ordinary differential equations:

$$\begin{cases} \dot{x} = z, \\ \dot{y} = x - y, \\ \dot{z} = -4x^2 + 8xy + yz + \alpha, \end{cases} \tag{1}$$

where $x(t), y(t)$, and $z(t)$ are the state variables, and $\alpha \in \mathbb{R}$ is a real parameter that affects the qualitative behavior of the system.
The first equation presents that z supplies the instantaneous time derivative of x, making it the primary driver of motion along the x-direction. Then the second equation shows linear negative feedback between x and y, causing y to stretched toward the value of x. The third equation is nonlinear, comprising a quadratic term in x, a bilinear interaction xy, a coupling term yz, and a constant bias, named α.

Make it together, these signs enable rich dynamics—including oscillations and chaos. The parameter α crucially shows the answer and is treated here as the primary bifurcation (control) parameter. In Jafari's original display, chaos below nonequilibrium conditions was noted, but a comprehensive global analysis was not pursued. To accomodate this, we systematically vary α and chart the associated bifurcation structures and also attractors. The sections that follow mix analytical fixed-point studies with numerical continuation to characterize equilibria, bifurcation scenarios, and the birth of both self-excited and hidden attractors.

3. Analytical Results

To check the qualitative dynamics of the nonlinear system (1), we start with an analytical study of its equilibria, local stability, and bifurcation structure. This gives the theoretical scaffolding for interpreting the numerical results. In particular, we locate and classify the equilibrium points, derive the characteristic polynomial of the linearized system, and also delineate the parameter intervals where stability changes occur via saddle–node and Hopf bifurcations.

3.1. Equilibrium Points

The equilibrium points of a dynamical system are the locations in wave space where all time derivatives vanish. To show the equilibrium points of system (1), we finish the algebraic equations obtained by setting the right-hand sides of the differential equations to zero such as:

$$\begin{cases} \dot{x} = z = 0, \\ \dot{y} = x - y = 0, \\ \dot{z} = -4x^2 + 8xy + yz + \alpha = 0. \end{cases} \tag{2}$$

The first equation yields $z = 0$. Substituting this into the third equation makes

$$-4x^2 + 8xy + \alpha = 0.$$

From the second equation we obtain $x = y$; changing this into the previous expression leads to

$$-4x^2 + 8x^2 + \alpha = 4x^2 + \alpha = 0,$$

which implies

$$x^2 = -\frac{\alpha}{4}. \tag{3}$$

This equation admits real solutions only when $\alpha \leq 0$. Thus, for $\alpha < 0$ the system possesses two symmetric equilibrium points:

$$E_{\pm}(\alpha) = \left(\pm\frac{\sqrt{-\alpha}}{2}, \pm\frac{\sqrt{-\alpha}}{2}, 0 \right). \tag{4}$$

When $\alpha > 0$, Eq. (3) has no real solutions, indicating that the system lacks equilibria within this parameter range.

In summary, the system undergoes a qualitative structural change at $\alpha = 0$: for $\alpha < 0$ two equilibria exist, whereas for $\alpha > 0$ no equilibrium is present. The case $\alpha = 0$ represents a degenerate situation in which the two equilibria coalesce at the origin of the phase space.

3.2. Local Stability Analysis

To examine the local behavior near an equilibrium, the system is linearized through the Jacobian matrix. The resulting linear system's eigenvalues determine local stability. If no eigenvalue has zero real part (the equilibrium is hyperbolic), the linearized system reproduces the qualitative dynamics of the nonlinear system in a neighborhood of the equilibrium [14].

Let the right-hand sides of system (1) be

$$f_1(x, y, z) = z, \qquad f_2(x, y, z) = x - y, \qquad f_3(x, y, z) = -4x^2 + 8xy + yz + \alpha,$$

with $\alpha \in \mathbb{R}$. The Jacobian matrix is

$$J(x, y, z) = \begin{pmatrix} 0 & 0 & 1 \\ 1 & -1 & 0 \\ -8x + 8y & 8x + z & y \end{pmatrix}. \tag{5}$$

Let $c = \pm\frac{\sqrt{-\alpha}}{2}$ for $\alpha < 0$; then the Jacobian evaluated at equilibrium becomes

$$J(c, c, 0) = \begin{pmatrix} 0 & 0 & 1 \\ 1 & -1 & 0 \\ 0 & 8c & c \end{pmatrix}. \tag{6}$$

Expanding the determinant of $(J - \lambda I)$ along the first row gives

$$\begin{aligned}
\det(J - \lambda I) &= \begin{vmatrix} -\lambda & 0 & 1 \\ 1 & -1-\lambda & 0 \\ 0 & 8c & c-\lambda \end{vmatrix} \\
&= (-\lambda)\begin{vmatrix} -1-\lambda & 0 \\ 8c & c-\lambda \end{vmatrix} - 0 \cdot \begin{vmatrix} 1 & 0 \\ 0 & c-\lambda \end{vmatrix} + 1 \cdot \begin{vmatrix} 1 & -1-\lambda \\ 0 & 8c \end{vmatrix} \\
&= (-\lambda)\Big[(-1-\lambda)(c-\lambda) - 0 \cdot 8c\Big] + \Big[1 \cdot 8c - (-1-\lambda)\cdot 0\Big] \\
&= (-\lambda)\,(-1-\lambda)(c-\lambda) + 8c \\
&= (-\lambda)\Big(\lambda^2 + (1-c)\lambda - c\Big) + 8c \\
&= -\lambda^3 + (c-1)\lambda^2 + c\lambda + 8c \\
&= -\Big(\lambda^3 + (1-c)\lambda^2 - c\lambda - 8c\Big).
\end{aligned}$$

which yields the cubic characteristic polynomial

$$\lambda^3 + (1-c)\lambda^2 - c\lambda - 8c = 0. \tag{7}$$

Denote the coefficients as

$$a_1 = 1 - c, \qquad a_2 = -c, \qquad a_3 = -8c.$$

Using the Routh–Hurwitz criterion [29], the necessary and sufficient conditions for local asymptotic stability are

$$a_1 > 0, \quad a_3 > 0, \quad a_1 a_2 > a_3.$$

These yield

$$c < 1, \qquad c < 0, \qquad c^2 + 7c > 0,$$

which are satisfied simultaneously only when $c < -7$. Because $c = -\frac{\sqrt{-\alpha}}{2}$, stability requires

$$\frac{\sqrt{-\alpha}}{2} > 7 \quad \Rightarrow \quad \alpha < -196.$$

Therefore, the negative equilibrium point

$$E_-(\alpha) = \left(-\frac{\sqrt{-\alpha}}{2}, -\frac{\sqrt{-\alpha}}{2}, 0\right)$$

is locally asymptotically stable if and only if $\alpha < -196$. The positive equilibrium E_+, corresponding to $c > 0$, violates $a_3 > 0$ and is thus unstable for all admissible α.

Such bifurcation-driven transitions between stability and oscillation commonly appear in feedback-controlled mechanical or electrical oscillators, underscoring the physical relevance of the present model.

3.3. Bifurcation Analysis

The local stability analysis above shows that the system admits a pair of symmetric equilibria of the form $(c, c, 0)$ with $c = \pm\frac{\sqrt{-\alpha}}{2}$. The negative equilibrium $E_-(\alpha)$ is locally asymptotically stable if and only if $\alpha < -196$. As α increases, the equilibrium gradually loses stability and eventually disappears for $\alpha \geq 0$. This behavior suggests the occurrence of bifurcations—qualitative changes in the system dynamics as α passes through critical values.

Theorem 1 (Bifurcation Structure of the System)**.** *Consider system* (1) *with parameter* $\alpha \in \mathbb{R}$*. The following bifurcation phenomena occur:*

(i) For $\alpha < 0$*, two symmetric real equilibria exist as in Eq.* (4)*. As* $\alpha \to 0^-$*, these equilibria approach each other and coalesce at the origin.*

(ii) At the critical value $\alpha = 0$*, the system undergoes a saddle–node bifurcation: the two equilibria merge into a degenerate point at the origin. No real equilibrium exists for* $\alpha > 0$*.*

(iii) As α *decreases further, a Hopf bifurcation occurs at* $\alpha = -196$*. At this point the Jacobian at* $E = (-7, -7, 0)$ *possesses a pair of purely imaginary eigenvalues, signaling a loss of stability and the onset of oscillatory motion.*

(iv) The Hopf bifurcation is supercritical: as α *increases past* -196*, a stable limit cycle bifurcates from the equilibrium while the equilibrium itself becomes unstable.*

Proof. From the equilibrium condition (3), real solutions exist only if $\alpha \leq 0$. For $\alpha < 0$ two symmetric equilibria exist; at $\alpha = 0$ they merge at the origin, and for $\alpha > 0$ none remain—characterizing a saddle–node bifurcation at $\alpha = 0$.

To analyze the Hopf bifurcation, substitute $\lambda = i\omega,\ \omega \in \mathbb{R}$ into Eq. (7):

$$(i\omega)^3 + (1-c)(i\omega)^2 - c(i\omega) - 8c = 0 \iff -i\omega^3 - (1-c)\omega^2 - ic\omega - 8c = 0.$$

Separating real and imaginary parts gives

$$\begin{aligned} \text{Real: } & -(1-c)\omega^2 - 8c = 0, \\ \text{Imaginary: } & -\omega^3 - c\omega = 0 \ \Rightarrow\ \omega^2 = -c. \end{aligned}$$

Substituting $\omega^2 = -c$ into the real part yields

$$-(1-c)(-c) - 8c = c(1-c) - 8c = -c^2 - 7c = 0,$$

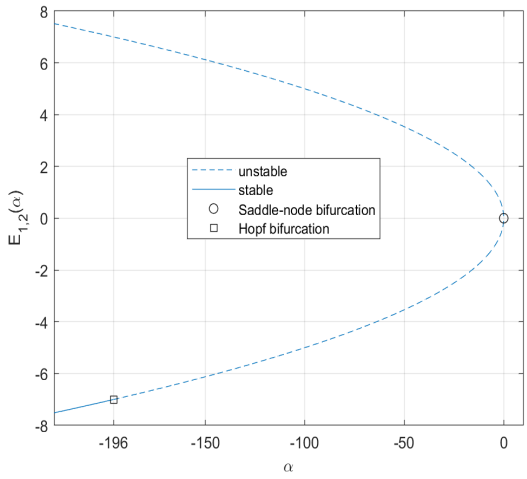

Figure 1: Variation of the real parts of the eigenvalues of $J(c, c, 0)$ with the control parameter α. Stable (negative real parts) for $\alpha < -196$ at E_-, unstable otherwise.

so $c = 0$ or $c = -7$. Because $c = 0$ implies $\omega = 0$, we take $c = -7$, corresponding to $\alpha = -4c^2 = -196$.

At this critical value, the Jacobian has a pair of purely imaginary eigenvalues $\lambda = \pm i\sqrt{7}$ satisfying the non-degeneracy condition for a Hopf bifurcation.

To determine its type, we compute the first Lyapunov coefficient ℓ_1, which governs the direction and stability of bifurcating periodic orbits. Following the normal-form theory and center-manifold reduction [11, 14],

$$\ell_1 = \frac{1}{2\omega_0}\Re\big\langle p,\, C(q,\bar{q},q) - 2B\big(q, A^{-1}B(q,\bar{q})\big) + B\big(\bar{q}, (2i\omega_0 I - A)^{-1}B(q,q)\big)\big\rangle\,, \tag{8}$$

where A is the Jacobian at equilibrium, ω_0 the imaginary part of the eigenvalues $\pm i\omega_0$, q and p the corresponding right and left eigenvectors normalized by $\langle p, q\rangle = 1$, and B and C the bilinear and trilinear forms derived from the second and third derivatives of f. Because system (1) is quadratic, $D^3 f(x) \equiv 0$ and the expression reduces to

$$\ell_1 = \frac{1}{2\omega_0}\Re\big\langle p,\, -2B\big(q, A^{-1}B(q,\bar{q})\big) + B\big(\bar{q}, (2i\omega_0 I - A)^{-1}B(q,q)\big)\big\rangle\,. \tag{9}$$

For $\alpha = -196$, where $E = (-7, -7, 0)$,

$$J(-7,-7,0) = \begin{bmatrix} 0 & 0 & 1 \\ 1 & -1 & 0 \\ 0 & -56 & -7 \end{bmatrix}.$$

The right eigenvector $q \in \mathbb{C}^3$ for $\lambda = i\sqrt{7}$ is

$$q = \begin{bmatrix} \frac{7}{142} - \frac{15i\sqrt{7}}{994} \\ -\frac{1}{142} - \frac{4i\sqrt{7}}{497} \\ \frac{15}{142} + \frac{7i\sqrt{7}}{142} \end{bmatrix},$$

and the corresponding adjoint (left) eigenvector $p \in \mathbb{C}^3$ for $-i\sqrt{7}$ is

$$p = \begin{bmatrix} -(-7 + i\sqrt{7}) \\ i\sqrt{7}(-7 + i\sqrt{7}) \\ 1 \end{bmatrix},$$

normalized such that $\langle p, q \rangle = \bar{p}^T q = 1$.

The bilinear form $B(u, v) \in \mathbb{R}^3$, representing second-order interactions of the vector field, is constructed from the Hessian matrices H_i of each component f_i evaluated at equilibrium:

$$B_i(u, v) = \frac{1}{2} \sum_{j=1}^{3} \sum_{k=1}^{3} \frac{\partial^2 f_i}{\partial x_j \partial x_k}(x_0)\, u_j v_k, \qquad i = 1, 2, 3,$$

so that

$$B(u, v) = \frac{1}{2} \begin{bmatrix} u^\top H_1 v \\ u^\top H_2 v \\ u^\top H_3 v \end{bmatrix}, \quad H_3 = \begin{bmatrix} -8 & 8 & 0 \\ 8 & 0 & 1 \\ 0 & 1 & 0 \end{bmatrix},$$

while H_1 and H_2 are zero matrices because the first and second equations are linear.

Numerical evaluation yields

$$\ell_1 \approx -0.00387599.$$

Because $\ell_1 < 0$, the system undergoes a supercritical Hopf bifurcation at $\alpha = -196$: as α increases beyond this value, a stable limit cycle emerges and the equilibrium becomes unstable. This transition is consistent with Fig. 1.

Supercritical Hopf bifurcations may lead to chaos through successive period-doubling bifurcations as the parameter α increases beyond the critical value -196. Therefore, it is natural to continue the analysis numerically to track how the periodic orbits evolve with changing α, thereby revealing the detailed route from simple oscillations to complex chaotic dynamics.

4. Numerical Continuation

To complement the analytical results, we perform numerical continuation by tracking the sequence of local maxima of $x(t)$ (denoted x_s) after discarding transients. This procedure yields parameter–response diagrams that reveal qualitative changes in the attractor as the control parameter α varies.

The ODEs are integrated with a fixed–step fourth–order Runge–Kutta (RK4), time step $\Delta t = 10^{-3}$, and total simulated time $t_{\max} = 6 \times 10^4$. Transients of length $t_{\mathrm{tr}} = 5 \times 10^4$ are discarded before sampling local maxima. Local maxima are detected when $\dot{x}$ changes sign from positive to negative with tolerance $|\dot{x}| < 10^{-8}$; the last 200 peaks are retained per α. Maximal Lyapunov exponents are computed via the Wolf–Swift–Swinney–Vastano algorithm [20], with QR re-orthonormalization every $\tau_{\mathrm{GS}} = 1.0$, horizon $T_{\mathrm{LE}} = 2 \times 10^5$ after

discarding $t_{\mathrm{tr,LE}} = 10^4$. Results are step-size robust for $\Delta t \in \{5 \times 10^{-4}, 10^{-3}, 2 \times 10^{-3}\}$. All computations are implemented in PYTHON.

For $\alpha < 0$, initial data are chosen at the negative equilibrium E_- obtained analytically (trajectories near E_- converge to periodic orbits for $\alpha \in [-196, 0]$). This choice follows the warm start concept, where the initial conditions are based on a previously known equilibrium point. This strategy helps speed up the convergence by starting the numerical simulation close to the expected solution, avoiding unnecessary exploration of the state space and reducing the computation time.

To quantify the chaotic behavior of the system, we also compute the Kaplan-Yorke dimension, which gives us the fractal dimension of the attractor. The Kaplan-Yorke dimension is computed based on the system's Lyapunov exponents, which measure the rate of separation of nearby trajectories in phase space. The Kaplan-Yorke dimension D_{KY} is calculated using the following formula:

$$D_{\mathrm{KY}} = m + \frac{\sum_{i=1}^{m} \lambda_i}{|\lambda_{m+1}|}$$

where $\lambda_1, \lambda_2, \ldots, \lambda_m$ are the Lyapunov exponents, ordered from largest to smallest, then m is the largest integer such that the sum of the first m exponents is positive, and λ_{m+1} is the first negative Lyapunov exponent, if it exists.

The Kaplan-Yorke dimension quantifies the degree of chaos in the system, and for chaotic systems, the dimension is often non-integer. A higher value of the dimension indicates greater complexity and fractal behavior. For our system, we calculated the Lyapunov exponents first, then used the Kaplan-Yorke formula to determine the dimension of the attractor. This provided a more precise understanding of the system's chaotic nature across different values of α.

Although a Hopf bifurcation is predicted analytically at $\alpha = -196$, sustained oscillations are first observed numerically near $\alpha \approx -31$. This offset reflects global nonlinear effects outside the local center-manifold neighborhood. In that regime, the system undergoes a period-doubling cascade as α increases, culminating in chaos.

Bifurcation diagrams

Figure 2 displays the bifurcation structure obtained from successive local maxima of $x(t)$. For $\alpha \in [-38, 0]$ [Fig. 2(a)] we observe a classical Feigenbaum-type cascade, interspersed with narrow periodic windows indicating intermittency and a tangled phase-space geometry. In contrast, for $\alpha \in (0, 0.8)$ [Fig. 2(b)] higher-order periodic motions collapse to lower periods via *period-halving*, a signature of the hidden-attractor regime in the absence of equilibria.

As seen in the bifurcation diagrams, the transition from periodic to chaotic behavior is governed by critical values of the control parameter α. This bifurcation behavior is further validated by the Lyapunov exponents, which help us characterize the system's chaos.

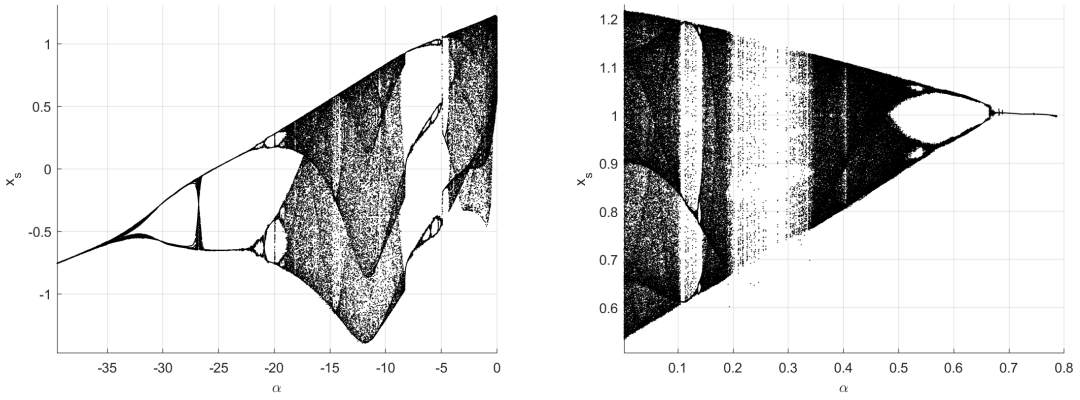

(a) (b)

Figure 2: Bifurcation diagrams from the last 200 local maxima of $x(t)$. (a) Period-doubling cascade with periodic windows for $\alpha \in [-38, 0]$. (b) Reverse period-halving for $\alpha \in (0, 0.8)$ characteristic of the hidden-attractor regime.

Maximal Lyapunov exponents

Figure 3 reports the maximal Lyapunov exponent $L_1(\alpha)$, which is a key indicator of chaos in dynamical systems. For $\alpha < 0$ [Fig. 3(a)], we observe that intervals where $L_1 > 0$ confirm chaotic behavior, while zeros correspond to periodic or quasi-periodic dynamics. A sharp rise in L_1 near $\alpha \approx -20$ marks the onset of robust chaos, followed by periodic windows where L_1 returns to zero or negative values, consistent with the transitions seen in the bifurcation diagram for $\alpha \in [-38, 0]$ [Fig. 2(a)]. For $\alpha > 0$ [Fig. 3(b)], L_1 decreases as α increases, following the trend of period-halving observed in the bifurcation diagram for $\alpha \in (0, 0.8)$ [Fig. 2(b)]. This decrease in L_1 signifies a simplification of the dynamics as the system approaches the hidden-attractor regime, where no equilibrium points exist and the system exhibits complex behavior without traditional attractors.

Kaplan–Yorke dimension

Figure 4 shows the Kaplan–Yorke (Lyapunov) dimension $D_{\mathrm{KY}}(\alpha)$, which is computed from the Lyapunov spectra and provides a measure of the complexity and fractality of the attractor.

For $\alpha < 0$ [Fig. 4(a)], D_{KY} increases from nearly 1 (indicating limit cycles) to non-integer values in the chaotic intervals. This increase corresponds to the transition into chaotic behavior, where the attractor becomes more complex and fractal. These changes in D_{KY} mirror the bifurcation diagram in Fig. 2(a), showing the period-doubling cascade.

For $\alpha > 0$ [Fig. 4(b)], D_{KY} decreases as α increases. This decrease in dimension reflects the simplification of dynamics as the system enters the hidden-attractor regime. The drop in D_{KY} corresponds to the period-halving seen in Fig. 2(b), where the attractor becomes less complex and more ordered.

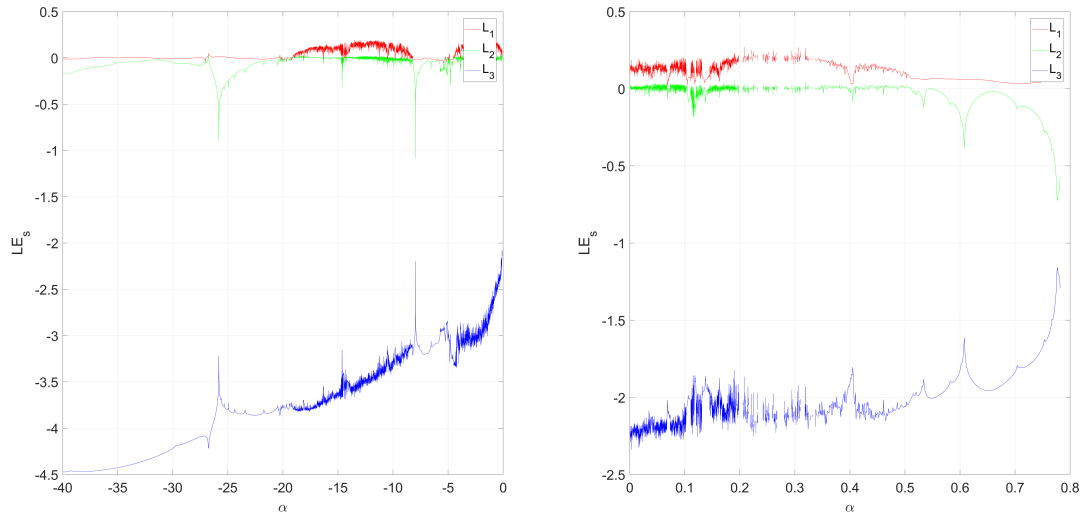

(a) (b)

Figure 3: Maximal Lyapunov exponent L_1 versus α. (a) For $\alpha \in [-38, 0]$, positive values certify chaos and dips to zero indicate periodic windows. (b) For $\alpha \in (0, 0.8)$, a gradual decrease in L_1 accompanies period-halving.

Representative phase portraits

Finally, Fig. 5 illustrates typical attractors across α. Panel (a) shows a periodic limit cycle at $\alpha = -50$; (b) captures the onset of period doubling near $\alpha = -31$; (c)–(d) display developed and fully developed chaotic motion ($\alpha = -17$ and -9); (e) depicts the transition region as equilibria approach disappearance ($\alpha = -1$); and (f) shows a hidden chaotic attractor at $\alpha = 0.1$, where equilibria are absent. Axes are (x, y, z); fonts and line widths are standardized across panels, and red markers indicate equilibria when present.

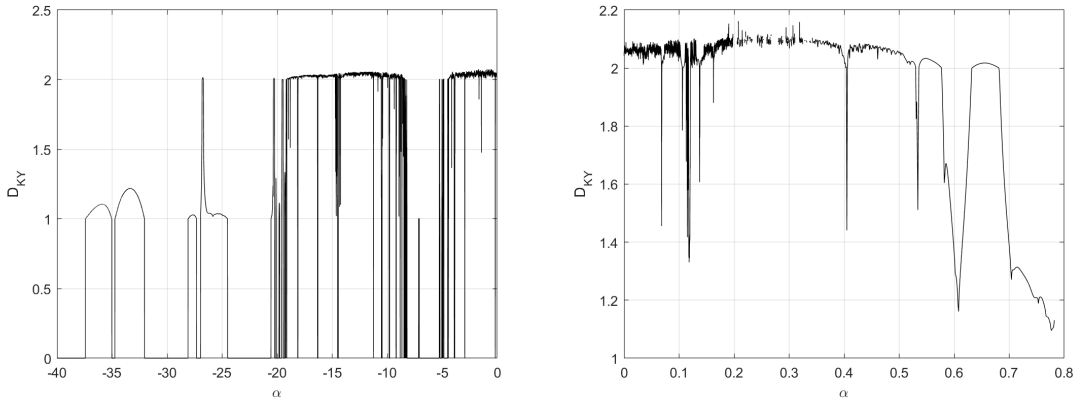

(a) (b)

Figure 4: Kaplan–Yorke dimension D_{KY} versus α. (a) Increase to non-integer values signals chaotic attractors for $\alpha \in [-38, 0]$. (b) Decrease with α for $\alpha \in (0, 0.8)$ is consistent with period-halving and reduced complexity.

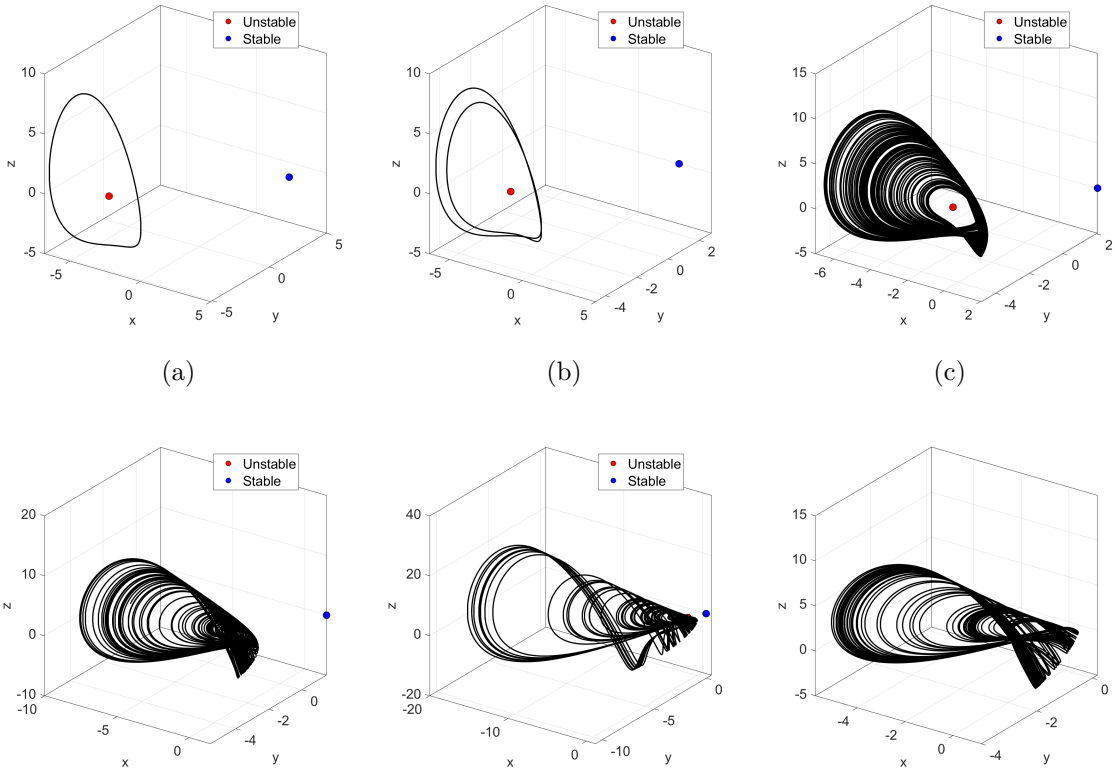

(a) (b) (c)

(d) (e) (f)

Figure 5: Representative phase portraits across α: (a) periodic limit cycle at $\alpha = -50$; (b) onset of period doubling at $\alpha = -31$; (c) developed chaotic motion at $\alpha = -17$; (d) fully developed chaos at $\alpha = -9$; (e) transition region as equilibria approach disappearance at $\alpha = -1$; (f) hidden chaotic attractor for $\alpha = 0.1$ where equilibria are absent. Red markers denote equilibria when present; axes are (x, y, z).

5. Conclusion

This work presented a hybrid analytical numerical study of a quadratic three dimensional system that displays two qualitatively distinct dynamical regimes organized by the control parameter α. Analytically, we proved that for $\alpha < 0$ the system possesses two symmetric equilibria which coalesce at the origin via a saddle–node bifurcation at $\alpha = 0$, and that the negative equilibrium undergoes a supercritical Hopf bifurcation at $\alpha = -196$ (first Lyapunov coefficient $\ell_1 < 0$), giving rise to a stable limit cycle. Global continuation and time–series diagnostics then revealed how these local instabilities scaffold the transition to complex behavior: for $\alpha \in [-21, 0]$ the system follows a period–doubling cascade to chaos, as confirmed by a positive maximal Lyapunov exponent and a non-integer Kaplan–Yorke dimension. In sharp contrast, for $\alpha > 0$ no equilibria exist, yet the flow sustains long-term oscillations through hidden attractors; their presence is supported by sensitivity and basin-selection experiments showing convergence to bounded chaotic motions from sets of initial conditions not connected to any equilibrium. Moreover, as α increases in $(0, 0.8)$ we observe a reverse trend—a period–halving sequence—indicating a distinct global organization of invariant sets in the equilibrium-free regime.

Conceptually, the paper unifies *self-excited* dynamics (when equilibria exist and lose stability) and *hidden* dynamics (when no equilibria are present and basins are disconnected from equilibria) within a single minimalist model, and methodologically couples normal-form analysis with numerical continuation and Lyapunov-spectrum-based validation. This dual perspective clarifies the route-to-chaos mechanisms on each side of $\alpha = 0$ and highlights how local bifurcations interface with global phase-space geometry. While the evidence for hidden attractors is primarily numerical, a rigorous characterization of basin geometry and possible multistability for $\alpha > 0$ remains open. Future work will therefore focus on codimension-two analysis around $\alpha \in 0, -196$, systematic basin cartography using grid-based or set-oriented methods, testing robustness under noise and parameter uncertainty, and exploring hardware implementations or control strategies (e.g., chaos suppression or targeting) inspired by the two-regime organization reported here.

Acknowledgements

The author would like to express sincere gratitude to Universitas Diponegoro for the financial support provided through the Non-State Budget Funding Scheme (Dana selain APBN) for Fiscal Year 2025, based on the Decree of the Head of the Institute for Research and Community Service of Universitas Diponegoro (LPPM), Number: 610/UN7.D2/HK/III/2025, dated March 18, 2025, and Contract Agreement Number: 222-179/UN7.D2/PP/IV/2025 dated April 8, 2025. This support was invaluable in facilitating and completing this study.

References

[1] T. Wang, Z. Luo, S. Zhang, and Z. Yu. Feedback-induced nonlinear spin dynamics in an inhomogeneous magnetic field. *Communications Physics*, 8(1):41, 2025.

[2] S. Suweis, F. Ferraro, C. Grilletta, S. Azaele, and A. Maritan. Generalized lotka–volterra systems with time correlated stochastic interactions. *Physical Review Letters*, 133(16):167101, 2024.

[3] T. S. Amer, M. A. Bek, and M. K. Abouhmr. On the vibrational analysis for the motion of a harmonically damped rigid body pendulum. *Nonlinear Dynamics*, 91:2485–2502, 2018.

[4] M. F. Ansori, N. Y. Ashar, and H. K. Fata. Logistic map-based banking loan dynamics with central bank policies. *Journal of Applied Nonlinear Dynamics*, 14(3):561–574, 2025.

[5] C. Guenoune, A. Bachmar, and S. Boutechebak. A dynamic problem with wear involving thermoviscoelastic materials with a long memory. *Nonlinear Dynamics & Systems Theory*, 24(5), 2024.

[6] Steven H. Strogatz. *Nonlinear Dynamics and Chaos: With Applications to Physics, Biology, Chemistry, and Engineering*. CRC Press, 2015.

[7] J. Chen, G. DeGrandi-Hoffman, V. Ratti, and Y. Kang. Review on mathematical modeling of honeybee population dynamics. *Mathematical Biosciences and Engineering*, 18(6), 2021.

[8] Z. Duan, H. Li, S. He, Y. Long, X. Yu, and Q. Ke. Integrated circuit of a chua's system based on the integral-differential nonlinear resistance with multi-path voltage-controlled oscillator. *Micromachines*, 15(3):401, 2024.

[9] A. Chakraborty and P. Veeresha. Effects of global warming, time delay and chaos control on the dynamics of a chaotic atmospheric propagation model within the frame of caputo fractional operator. *Communications in Nonlinear Science and Numerical Simulation*, 128:107657, 2024.

[10] C. Liu, S.-K. Lai, Y.-Q. Ni, and L. Chen. Dynamic modelling and analysis of a physics-driven strategy for vibration control of railway vehicles. *Vehicle System Dynamics*, pages 1–31, 2024.

[11] Yuri A. Kuznetsov. *Elements of Applied Bifurcation Theory*. Springer, New York, 3 edition, 2004.

[12] V. I. Arnold. Bifurcations of equilibria. In *Dynamical Systems V*, pages 1–8. Springer, Berlin, 1994.

[13] Lawrence Perko. *Differential Equations and Dynamical Systems*, volume 7 of *Texts in Applied Mathematics*. Springer, New York, 2013.

[14] Stephen Wiggins. *Introduction to Applied Nonlinear Dynamical Systems and Chaos*. Texts in Applied Mathematics. Springer, New York, 2003.

[15] N. Ananthkrishnan, N. K. Gupta, and N. K. Sinha. Computational bifurcation analysis of multiparameter dynamical systems. *Journal of Guidance, Control, and Dynamics*, 32(5):1505–1513, 2009.

[16] M. di Bernardo, C. Budd, A. R. Champneys, P. Kowalczyk, A. Nordmark, G. Oli-

var Tost, and P. T. Piiroinen. Bifurcations in nonsmooth dynamical systems. *SIAM Review*, 50(4):629–701, 2008.

[17] Y. Han, Q. Cao, and J. Ji. Nonlinear dynamics of a smooth and discontinuous oscillator with multiple stability. *International Journal of Bifurcation and Chaos*, 25(14):1550038, 2015.

[18] J. C. Sprott. Some simple chaotic flows. *Physical Review E*, 50(2):647–650, 1994.

[19] S. Jafari, J. C. Sprott, and S. M. R. Hashemi Golpayegani. Elementary quadratic chaotic flows with no equilibria. *Physics Letters A*, 377(9):699–702, 2013.

[20] A. Wolf, J. B. Swift, H. L. Swinney, and J. A. Vastano. Determining lyapunov exponents from a time series. *Physica D*, 16(3):285–317, 1985.

[21] J. Nichols, R. D. Guy, and B. Thomases. Period-doubling route to chaos in viscoelastic kolmogorov flow. *Physical Review Fluids*, 10:L041301, 2025.

[22] S. Saju, K. Kinashi, N. Tsutsumi, W. Sakai, and B. J. Jackin. Period-doubling route to chaos in photorefractive two-wave mixing. *Photonics*, 11:521, 2024.

[23] X. Zhang et al. From breather solitons to chaos in an ultrafast laser. *Chaos, Solitons & Fractals*, 182:114841, 2024.

[24] Z. Rashidi, S. Azizi, and O. Rahmani. Period-doubling cascade route to chaos in an initially curved microbeam resonator exposed to fringing-field electrostatic actuation. *Nonlinear Dynamics*, 112:9915–9932, 2024.

[25] M.-F. Danca. Chaotic hidden attractor in a fractional order system modelling the interaction between dark matter and dark energy. *Communications in Nonlinear Science and Numerical Simulation*, 131:107838, 2024.

[26] S. Roy, A. Ray, and A. Roy Chowdhury. Kosambi–cartan–chern perspective on chaos: Unveiling hidden attractors in nonlinear autonomous systems. *Physical Review E*, 109:044205, 2024.

[27] X. Hu, S. Wang, P. Wu, H. Cao, and X. Zhang. Self-excited and hidden multi-scroll attractors in a novel extremely simple three-dimensional system. *Chinese Journal of Physics*, 2025. In press.

[28] V. Varshney, S. Leo Kingston, S. Srinivasan, and S. Kumarasamy. Hidden attractors in fractional-order discrete maps. *The European Physical Journal B*, 97:161, 2024.

[29] A. Hastir and R. Muolo. A generalized routh–hurwitz criterion for the stability analysis of polynomials with complex coefficients: Application to the pi-control of vibrating structures. *IFAC Journal of Systems and Control*, 26:100235, 2023.